Development of control strategies for novel systems of a full-scale OWC for the WEDUSEA project

James Kelly, Tony Lewis, Sean Barrett, Juncal Guerrero Muñoz, Cristina González Perancho,

Melanie Hau, Fabian Bonnet

Abstract—**The Wave Energy Demonstration at Utility Scale to Enable Arrays (WEDUSEA) project is a joint venture between 14 partners spanning industry and academia from Ireland, the UK, France, Germany, and Spain. The main goal of the project it to deploy a 1 MW OE35 oscillating water column wave energy converter in Orkney, Scotland, UK for 2 years. The project is testing new advances in the power take-off (PTO) system of the OE35. The new additions to the OE35 platform are a Wells turbine, 4 pressure relief valves in parallel of the turbine, and a super capacitor-based Energy Storage System. To fully realise the new components of the PTO, new control algorithms must be developed for each new subsystem. To help with development and testing of the control algorithms, a wave-to-wire mathematical model of the new OE35 system was designed and built using MATLAB Simulink-SimScape. The model has been used to assist with developing early-stage algorithms for each new system.**

Keywords— **Wave energy, Oscillating water column, Control, Power Quality, Wave-to-wire model**

I. Introduction

THE WEDUSEA project is a €19.6 million European wide joint venture between 14 partners spanning industry and academia from Ireland, the UK, France, Germany, and Spain that will culminate with a two-year, grid connected deployment of a 1MW rated oscillating water column (OWC) wave energy converter (WEC) at the EMEC test site in Orkney, Scotland, UK. The WEDUSEA deployment will be the second deployment of the OE35 buoy. The first deployment of the OE35 will be at the US Navy Wave Energy Test Site (WETS) in Kāne'ohe Bay, O'ahu, Hawaii, USA during the summer of 2023 [1].

The WEDUSEA project has three primary goals. The first is demonstrate that wave technology is on a cost reduction trajectory, and thus stimulate larger commercial array scale up and further industrialisation, through de-risking larger scale investments. This will therefore help meet the 1 GW target set out in the 2030 DG-ENER Offshore Renewable Energy Strategy and the 2050 EU renewable energy targets. The second is to boost the development of the wave energy industry worldwide by creating awareness of the potential of wave energy amongst policy makers, industry, potential investors and the public, thus directly impacting policy, public perception and investor confidence in wave energy. The third primary objective of WEDUSEA is to disseminate results and outcomes which enable the capitalisation and exploitation of the results through new innovations, products and services, as well as feeding both environmental databases and worldwide technical standards.

As part of that first goal, the project will introduce several novel systems and control strategies to the OE35 device to improve performance, annual power production, and grid integration, which will help further cost reduction. During the initial planning and design phases of the project, a wave-to-wire numerical model has been created to investigate the impact these new systems will have on device performance and allow for the testing and development of the control strategies necessary to operate the 1MW power take-off (PTO) system as efficiently as possible. This paper will detail the novel systems added to the OWC, the control strategies developed for the new additions, and the modelled performance of the OWC.

II. OE35 Novel Additions

The second deployment of the OE35 allows the opportunity to redesign subsystems of the device to improve overall system performance. The decision to redesign the subsystems was based on lessons learned from the WETS project and from improvements in the

James Kelly, Tony Lewis, and Sean Barrett are with Ocean Energy, 3 Casement Square, Cobh, Cork, Ireland (e-mail: jfk@oceanenergy.ie; tl@oceanenergy.ie; sb@oceanenergy.ie).

Juncal Guerrero Muñoz and Cristina González Perancho are with AST Ingeniería, Parque Científico y Tecnológico de Gijón, C/ Profesor Potter 126. 33203 Gijón, Asturias, Spain (e-mail: juncal@ast-ingenieria.com; cristina@ast-ingenieria.com).

Melanie Hau and Fabian Bonnet are with Fraunhofer Institute for Energy Economics & Energy System Technology IEE, Joseph-Beuys-Str. 8, 34117 Kassel, Germany (e-mail: melanie.hau@iee.fraunhofer.de; fabian.bonnet@iee.fraunhofer.de).

Digital Object Identifier: https://doi.org/10.36688/ewtec-2023-561

current state of the art. The additions to the OE35 for the WEDUSEA project Power Take-off (PTO) system include replacing an impulse turbine for a Wells turbine, the addition of airflow relief valves, and a super capacitor bank for short-term energy storage.

A. Pneumatic Power Take-off

The OE35 to be deployed at WETS uses an impulse-style turbine to convert the pneumatic energy to the mechanical energy that drives the electrical generator. For the EMEC deployment of the OE35, the impulse-style turbine is replaced with a Wells turbine. The goal in the design of the Well turbine was to achieve a design capable of producing 1 MW of mechanical output with a peak efficiency close to 75%.

Along with the Wells turbine, there will be 4 relief valves mounted in parallel with the turbine. The valves are of varying diameters and together with the Wells turbine comprise the pneumatic-to-mechanical stage of the PTO system.

The use of a single relief valve has been utilised at the Pico OWC in the Azores to help regulate pneumatic power and avoid turbine stall, and it led to a significant increase in power production through stall avoidance [2, 3]. For WEDUSEA, the decision made was to allow for a maximum of 1.5 MW of pneumatic power in the turbine (around 1MW of mechanical power) and 3MW of pneumatic power in the chamber. The valves are designed to decrease the pressure in the chamber, which in turn releases 1.5 MW. The addition of the relief valves will allow the system to operate in larger energy sea states while avoiding both aerodynamic stall and over taxing of the turbine-generator system. The valves are staggered in size to allow the flow control system up to 16 different variations. The potential final turbine and relief valve set up is shown in Fig. 1.

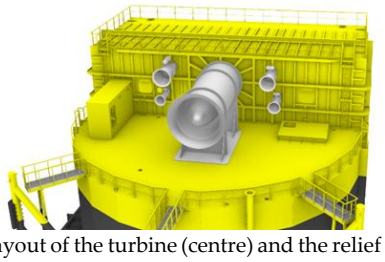

Fig. 1: The layout of the turbine (centre) and the relief valves (2 left, 2 right) for the WEDUSEA project.

B. Electrical Power Take-off

The other novel addition to the OE35 system is the introduction of a super capacitor based short-term Energy Storage System (ESS). The electrical power produced by the wave energy system is fluctuating by nature. These fluctuations in power can have negative impacts on the power quality on the grid by creating voltage variations, such as flicker. The aim of the ESS is to buffer energy of this fluctuating power output of the wave energy converter. That way, the power feed-in to the electrical grid will be smoothed and flicker will be reduced. The WEDUSEA OWC ESS is an integral part of the electrical PTO where it is connected to the generator via the local DC-bus, as shown in Fig. 2. The power converter feeding the super capacitor allows for the ESS to be a fully controllable.

The primary objective of the super capacitor system is to absorb power peaks and use that stored energy to minimise energy troughs. The power output is aimed to be levelized by mitigating fluctuations in a certain frequency range. Along with the ability of the super capacitor to improve power delivery to the grid, the ESS may also facilitate improved performance and increased annual power production by the mechanical PTO by enhancing the turbine-generator control system flexibility.

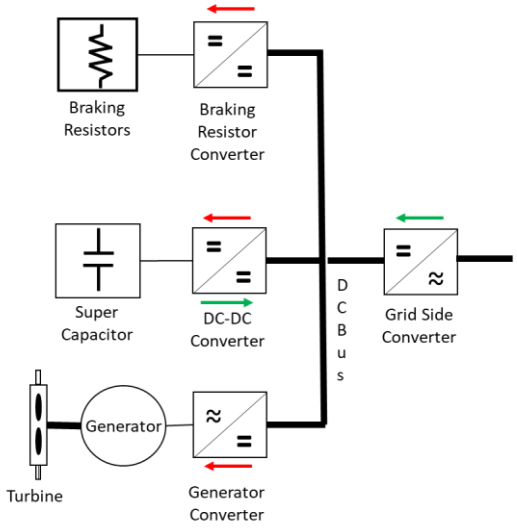

Fig. 2: The electrical PTO of the WEDUSEA project where the ESS is labelled as 'SuperCap' and 'SuperCap Converter'.

C. System Control Methodologies

To incorporate the bypass valves and the super capacitor into the WEDUSEA OWC, more complex algorithms will need to be created for control of the mechanical and electrical components of the PTO. During these early stages of control development, the turbine, valve, and ESS control algorithms are developed and operated separately.

The turbine control's primary function is to maximize the pneumatic-to-mechanical energy conversion. This includes avoiding aerodynamic stall of the turbine, while maximizing pneumatic-to-mechanical conversion efficiency. The turbine is controlled using the electrical generator by applying a reference braking torque to the generator via a power electronics converter. The primary inputs to the control algorithm for the turbine are chamber pressure and turbine angular velocity.

The valve control's primary function is to minimise aerodynamic stall of the turbine and allow the OE35 to operate in more energetic sea conditions that might typically send the device into shut down. They are controlled via a pneumatic system that is used to open and

close the valves as required. The main input to the valve control is internal chamber pressure. The valve control relies on a digital signal to open or close each valve independently. The travel time for each valve is different, with the smaller valves taking only 2-4 seconds to open and close, while the larger valves require between 10-20 seconds. These discrepancies in travel time result in different control approaches for the small and large valves.

The central goal of the ESS controller is to minimise the fluctuations of the power injected into the grid by the electrical PTO system while maintaining the voltage levels of the super capacitor bank. The initial control algorithm used to control power flow to the ESS relies on the measured output power of the generator, the period of the pressure fluctuations within the internal chamber of the OE 35, and the voltage level of the capacitor bank.

III. MATLAB Model Design

To help develop the control algorithms, a wave-to-wire model of the OE35 system was developed using MATLAB Simulink & SimScape. From the wave input through to the mechanical behaviour of the turbine, the model utilises Simulink. The turbine is directly coupled to the electrical generator, and from the generator to the grid, the model relies on SimScape electrical to model the electrical section of the PTO, which includes the power electronics controlling the generator-turbine and the power flow to the ESS and grid.

The model, shown in Fig. 3, replicates the complex interactions between the various stages of the energy conversion chain; with the left side containing the hydrodynamic through mechanical sections in Simulink and the right side including the SimScape electrical model of the electrical PTO. This section offers a brief summary of the mathematical model used.

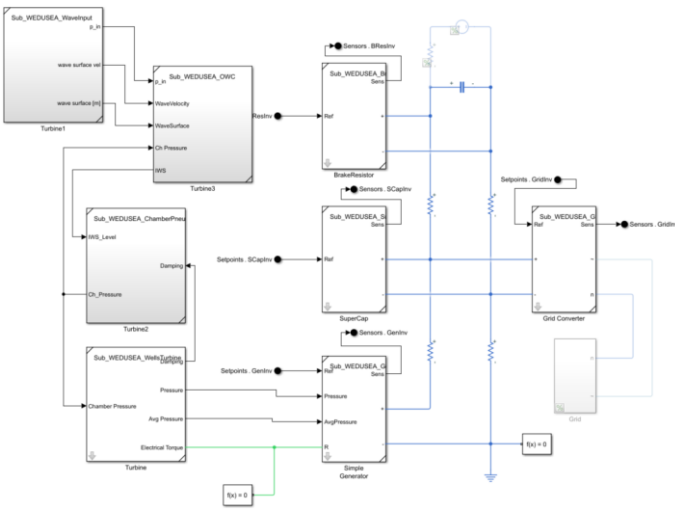

Fig. 3: Wave-to-wire MATLAB model of the OE35 PTO.

D. Wave Input Generation

The first stage of the model is generating the irregular sea waves that will be encountered at the deployment site at EMEC. The Bretschneider spectrum is used to provide a reasonable representation of the wave climate at the EMEC test site [4]. The wave input is thus created by selecting values for significant wave height, H_s, and peak period, T_P, and applying the Bretschneider spectrum to create the changing external water surface elevation, which represents the waves that interacts with the OE35.

E. Hydrodynamic, Pneumatic, & Mechanical Modelling

To determine the power absorbed by the passing waves, the hydrodynamic response of the OE35 is determined by applying the mathematical model presented in [5], which provides the motion of the changes of the internal water surface and the motion of the buoy itself.

However, the motions of the buoy and the internal water surface are also influenced by the pressure differential between the chamber and the atmosphere. The gauge pressure inside the chamber is calculated using (1) with minor changes [6].

$$\begin{cases} \frac{dV}{dt} + \frac{V}{\gamma p_0 + p}\frac{dp}{dt} + {}^{p}/_{k} = 0, & p \geq 0, \\ \left(1 + \frac{p}{\gamma p_0}\right)\frac{dV}{dt} + \frac{V}{\gamma p_0}\frac{dp}{dt} + {}^{p}/_{k} = 0, & p < 0 \end{cases} \tag{1}$$

Equation 1 is the original equation from [6], where V is volume, p is chamber gauge pressure, k is damping coefficient, p_0 is atmospheric pressure, and γ is the specific heat ratio of air. This model includes the linear damping from the Wells turbine, which is represented by p/k. The relief valves are represented as several orifices, which introduce a polynomial damping, so (1) had to be updated.

The linear damping of the Wells turbine is directly related to the rotational speed of the turbine, and a simple coefficient, k_D, multiplied by the rotational speed provides the damping value for the turbine, k_T. The value of k_D was determined through CFD modelling of the turbine designed for this project. The damping coefficients of the valves are simple orifice damping values determined by the diameter of the orifice with a discharge coefficient, C_D, which for the current model is assumed to be 0.6. To combine the damping of the turbine with that of the valves, the flow for each element is added together to determine the total flow through the OE35 system, as was applied in [2].

The final element of the equation on the left in (1) is replaced by

$$\begin{cases} Q_{Total} = \frac{p}{k_T} + \sqrt{\frac{p}{k_1}} + \sqrt{\frac{p}{k_2}} + \sqrt{\frac{p}{k_3}} + \sqrt{\frac{p}{k_4}}, p \geq 0, \\ Q_{Total} = \frac{p}{k_T} - \sqrt{\frac{-p}{k_1}} - \sqrt{\frac{-p}{k_2}} - \sqrt{\frac{-p}{k_3}} - \sqrt{\frac{-p}{k_4}}, p < 0. \end{cases} \tag{2}$$

where k_1 is damping coefficient of the valve 1, k_2 is damping coefficient of the valve 2, k_3 is damping coefficient of the valve 3, and k_4 is damping coefficient of the valve 4. Combining (1) and (2) results in

Equation (3) is solved for *dp/dt* and integrated to determine chamber pressure, and the chamber pressure is fed back into the hydrodynamic model where it influences the motion of the internal water surface and the buoy.

To determine the mechanical torque induced in the turbine, the flow across the turbine and the angular velocity of the turbine are combined to determine the turbine torque coefficient. The turbine characteristics from CFD modelling are combine with the torque coefficient to determine mechanical torque exerted on the turbine. These equations have been repeatedly proven including in [3].

F. Electrical Modelling

The electrical generator is modelled in the combination with its power electronics converters in a common way, which does not take the type of the generator into account. Modelling the system this way leads to a direct conversion of mechanical rotational energy into electrical DC energy. The part between converter and generator is not modelled directly since it depends on the type of generator, but it is modelled indirectly by assuming separate efficiency factors for converter and generator.

The main reason for this simplification is to maintain short simulation run times. In electrical systems, typically, small time constants occur, which require small simulation time steps to produce accurate calculations. This dissents to short simulation run times. To find a compromise on this problem, the electrical part between converter and generator was not modelled.

The DC-side of the combined generator-converter model is connected to a DC-Bus, which can be seen as a backbone for transferring electrical energy within the electrical PTO system. All other electrical main components are connected to this DC-Bus. This includes the grid-side converter for transferring energy to the public grid, the super capacitor DC-DC converter for smoothing power fluctuations and the braking resistor power converter.

The concept and basic modelling of the different converters is the same. Since the goal of the PTO-Model is to simulate power flow, system behaviour and development of operation control strategies, the focus on converter- and component-modelling lies on power transferring as fundamental size. Each power converter has two electrical interfaces that are modelled as ideal controlled current sources. To transfer power from one side to the other, converter control is implemented that measures voltage, current, and power on both sides of the converter. These signals then are used to maintain the power conservation law in every simulation time step. The converter control also ensures that the electrical signals do not exceed their specified limits.

As mentioned above, the modelling of the generator and its power converter was done in a combined model. Here, one side of the inverter represents the electrical side with voltage, current, and electrical power, while the other side

$$\begin{cases} \dfrac{dV}{dt} + \dfrac{V}{\gamma p_0 + p}\dfrac{dp}{dt} + Q_{Total} = 0, & p \geq 0, \\ \left(1 + \dfrac{p}{\gamma p_0}\right)\dfrac{dV}{dt} + \dfrac{V}{\gamma p_0}\dfrac{dp}{dt} - Q_{Total} = 0, & p < 0. \end{cases} \quad (3)$$

represents the mechanical side, modelled by torque, rotational speed, and mechanical power.

All power electronics converters can be controlled by direct power setpoint and additionally by other converter-specific setpoints, such as torque- or speed-controller for the combined generator-converter or voltage- and current-controllers for the electrical-only power converters. Internally, each controller translates the current control mode setpoint to a power value, which has to be transferred from one side to the other side of the power converter. The direction of power flow through each converter is determined by the sign of the power setpoint or by internal rules in case of other setpoint modes. Additionally, the power flow direction can be restricted if needed, e.g., to disallow feeding electrical energy from the public grid into the DC-Bus, if DC-Bus voltage is low and the grid converter is operated in DC-voltage control mode.

IV. Control Development, Simulations, & Results

G. Turbine Control

The electrical early development of the control focused on generator torque control, where the reference torque of the generator is set based on input parameters. The initial input parameters were selected as turbine rotational speed and average and instantaneous pressure inside the chamber. These initial input parameters were selected based on work that showed both methods to be simple and effective [7]. The basic equations for both approaches are shown below with (4) based on speed and (5) based on pressure.

$$\tau_{ref} = a_1\Omega^2 + a_2\Omega + a_3 \quad (4)$$

$$\tau_{ref} = b_1\bar{p} + b_2|p - \bar{p}| \quad (5)$$

where τ_{ref} is reference torque, Ω is rotational speed in rads/s, p is pressure, $\bar{p}$ is a moving average of chamber pressure, and a and b are constants determined from turbine characteristics extracted from CFD modelling.

These control algorithms were tested using the MATLAB Simulink-SimScape model over a range of sea states based on the scatter diagram for the EMEC test site where the OE35 will eventually be deployed. Table I shows the scatter diagram for EMEC, while Table II indicates the sea state conditions simulated during development of the turbine control algorithm. The initial turbine control algorithm testing was conducted only under conditions with an H_s of 3.5 m because in higher energy sea states, the relief valves will be required, and relief valve testing was carried out in a different phase of testing.

TABLE I
SCATTER DIAGRAM FOR EMEC TEST SITE

Hs/Tp	6	7	8	9	10	11	12	13	14	15	16
0	0.13%	0.39%	0.34%	0.25%	0.16%	0.05%	0.02%	0.01%	0.01%	0.00%	0.00%
0.5	1.02%	2.43%	3.47%	2.97%	2.20%	1.08%	0.67%	0.25%	0.12%	0.06%	0.07%
1	0.65%	1.82%	3.92%	4.45%	3.83%	2.27%	1.54%	0.73%	0.32%	0.15%	0.13%
1.5	0.66%	1.09%	2.12%	3.04%	3.92%	2.40%	1.86%	0.92%	0.49%	0.19%	0.13%
2	0.42%	0.81%	1.21%	1.88%	2.94%	2.48%	1.98%	1.06%	0.55%	0.19%	0.14%
2.5	0.09%	0.50%	0.79%	1.15%	1.90%	1.77%	1.66%	0.82%	0.50%	0.18%	0.11%
3	0.01%	0.19%	0.54%	0.83%	1.21%	1.19%	1.28%	0.85%	0.38%	0.17%	0.11%
3.5	0.00%	0.03%	0.28%	0.57%	0.87%	0.86%	1.01%	0.62%	0.34%	0.16%	0.11%
4	0.00%	0.00%	0.08%	0.35%	0.61%	0.59%	0.65%	0.48%	0.26%	0.12%	0.08%
4.5	0.00%	0.00%	0.01%	0.12%	0.46%	0.43%	0.49%	0.39%	0.20%	0.08%	0.06%
5	0.00%	0.00%	0.00%	0.03%	0.27%	0.37%	0.39%	0.26%	0.18%	0.09%	0.06%
5.5	0.00%	0.00%	0.00%	0.00%	0.11%	0.26%	0.26%	0.21%	0.12%	0.06%	0.04%
6	0.00%	0.00%	0.00%	0.00%	0.01%	0.13%	0.22%	0.16%	0.09%	0.04%	0.02%
6.5	0.00%	0.00%	0.00%	0.00%	0.00%	0.03%	0.14%	0.11%	0.06%	0.02%	0.01%
7	0.00%	0.00%	0.00%	0.00%	0.00%	0.01%	0.06%	0.09%	0.04%	0.02%	0.01%
7.5	0.00%	0.00%	0.00%	0.00%	0.00%	0.00%	0.02%	0.04%	0.03%	0.01%	0.01%
8	0.00%	0.00%	0.00%	0.00%	0.00%	0.00%	0.00%	0.03%	0.03%	0.01%	0.00%

TABLE II
SEA CONDITIONS APPLIED FOR TURBINE CONTROL DEVELOPMENT

H_s (m)	2.33	2.33	3.50	3.50	3.50	3.50
T_p (s)	6.11	13.76	7.64	9.16	11.46	15.27
SS#	B01	B18	B02	B04	B06	B12

The critical goal of the turbine control algorithms during this phase was to avoid aerodynamic stall, so that the system could operate without the use of the relief valves. By avoiding the use of the relief valves in lower energy sea conditions, the PTO will be able to maintain its maximum efficiency.

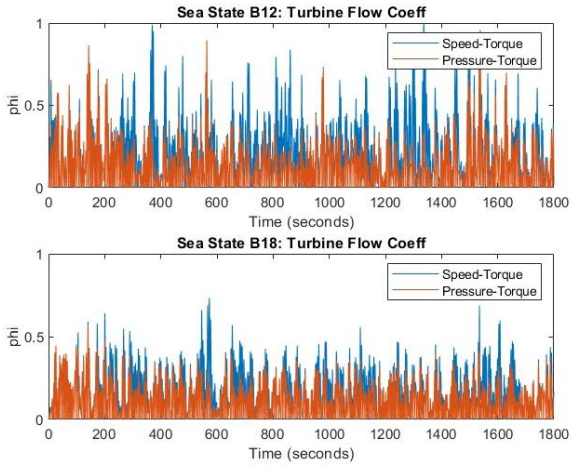

Fig. 4: Flow coefficient values during initial testing of speed and pressure-based control algorithm.

The flow coefficient, ϕ, for the turbine is used to determine if the turbine entered aerodynamic stall during modelling. At values of ϕ > 0.48, the Wells turbine being modelled in this system will enter stall. Fig. 4 above shows the values of ϕ for a 30-minute simulation under sea state conditions B12 and B18 with both the speed-torque and the pressure-torque control algorithms. In both tests shown and all 6 sea conditions tested, the turbine enters stall under either control algorithm, with the pressure-torque algorithm performing noticeable better. This is true even at the lowest energy sea states that the OE35 will operate under. These results indicate that the original algorithms chosen for turbine control are inadequate for controlling a Wells turbine. As the types of algorithms tested were initially developed for a bi-radial impulse turbine which does not encounter aerodynamic stall, this result is not unexpected, but the algorithms did provide a good starting point for control development.

The initial algorithms were repeatedly adjusted, first by adjusting the coefficients, then by adding additional inputs to the system. During further development and trials, it was determined that combining the two algorithms led to the best optimisation of the turbine performance.

The new algorithm inputs include pressure, average pressure, rotational speed, and a new term, optimum rotational speed. The optimum rotational speed is determined by average pressure and the turbine characteristics extracted from CFD modelling of the turbine. A moving speed floor was also added to the turbine control. The original control algorithms had a speed floor at the minimum speed of the generator, while the new hybrid algorithm as a moving speed floor based on the calculated optimum speed. Equation (6) is a mathematical representation of the updated hybrid algorithm.

$$\tau_{ref} = c_1\overline{p} + c_2|p-\overline{p}| * \left(\frac{\Omega-\Omega_{opt}}{\Omega_{opt}}\right); \quad \Omega_{opt} \geq c_3\Omega_{opt} \qquad (6)$$

The updated hybrid algorithm nearly eliminated hydrodynamic stall in each of the six sea states model tested during phase one testing. Fig. 5 shows the plots of ϕ again with the inclusion of the new hybrid algorithm, and in both simulations the turbine avoids aerodynamic with the new control algorithm.

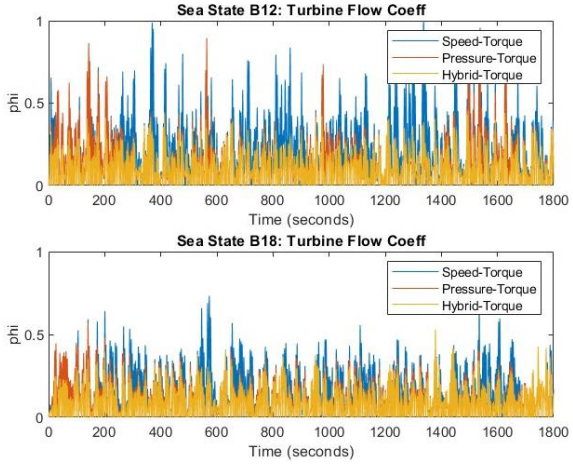

Fig. 5: Flow coefficient values during initial testing of hybrid control algorithm.

H. Relief Valve Control

With the turbine control algorithm developed to operate in the lower sea state conditions, the next stage in the control development for the OE35 was the operation of the relief valves. When controlling the relief valves, the goal is to keep the maximum pneumatic power in the turbine below 1.5 MW (1 MW of mechanical power approx.) Opening the valves during operation will both lower the overall pressure within the plenum chamber and allow a portion of the air flow to escape the chamber without passing through the turbine.

The CFD modelling of the turbine rotor indicates that for speeds above 1600 rpm the turbine will achieve approx. 1 MW of mechanical power when the pressure in the chamber is about 11 kPa. At this point the relief valves shall be opened, with the express goal to keep the maximum chamber pressure below 11 kPa.

Additional CFD testing was performed to determine how each valve, as well as combinations of valves, impacted chamber pressure and air flow through the turbine. Fig. 6 is an example of the CFD results. The pressure relief in the chamber was evaluated for different situations and set-ups. The pressure values were computed in the chamber for three different air flows going outside the turbine, considering all valves closed, one unique valve open or all valves open (as applicable). Table III below shows the results from tests with the flow set to 250 m^3/s.

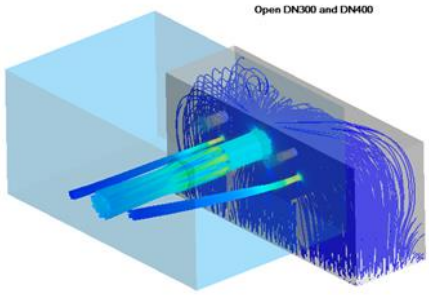

Fig. 6: CFD modeling of flow through the system with DN300 and DN400 open.

TABLE III
CFD VALVE TEST RESULTS WITH FLOWS SET TO 250 M^3/S

Measurement	Valves Closed	DM300 Open	DM400 Open	DM600 Open	DM800 Open
Max Hull Pressure (Pa)	20544	17960	16311	13521	11658
Pressure change ΔP Hull (Pa)	N/A	2584	4233	7023	8886
Volumetric Turbine Flow (m3/s)	276.43	258.75	247.92	228.92	215.06

Based on the CFD simulations, the pressures at which each valve should be opened and when they should be closed was determined. It was discovered from the CFD results that an individual valve will result in a consistent percentage of pressure drop within the plenum chamber when it is open, and this ratio can be used to determine the opening and closing of the valves. As a result, the opening and closing of the valves are based on the maximum pressure readings in the chamber.

The command to open or close a valve was based on a maximum pressure measured within the plenum chamber. Table IV shows the percentage of pressure released by opening an individual valve, along with pressure measurements that will result in opening or closing a valve as well as the stroke times for the opening and closing of each valve. To initiate the opening of a valve, a maximum pressure must be measured that falls above a valve's opening pressure while following below the next valves opening pressure, and this measurement must occur within a specific time window. Once a valve is open, it will not close again, unless a set period of time has elapsed where the maximum pressure never reaches the suggested closing pressure.

TABLE IV
OPENING AND CLOSING PRESSURE & STROKE TIMES FOR EACH VALVE

Valve	Pressure Release %	Opening Press (Pa)	Closing Press (Pa)	Opening Time (s)	Closing Time (s)
DM300	10	12000	5000	2.9	3.4
DM400	20	13000	6000	2.9	3.4
DM600	35	15000	10000	9	11
DM800	44	19000	14000	18	20

The valve control algorithms testing was carried out under sea states B05, B07, B08, B09, B13, and B15. The corresponding sea conditions for the sea states list above are provided in Table V. During simulation trials, it was discovered that the opening of valves as a pressure release had more significantly impacted the hydrodynamic response than initially anticipated. While the opening of the valves did lower the pressure in the plenum chamber, the lower pressures resulted in increased movement of internal water surface and thereby increased flow. This resulted in the anticipated pressures and flows shown in modelling to be much larger than those determined during CFD modelling.

TABLE V
SEA CONDITIONS APPLIED FOR VALVE CONTROL DEVELOPMENT

H_s (m)	5.83	5.83	8.75	5.83	5.83	8.17
T_p (s)	9.16	11.46	11.46	13.76	15.27	19.10
SS#	B05	B07	B08	B09	B15	B13

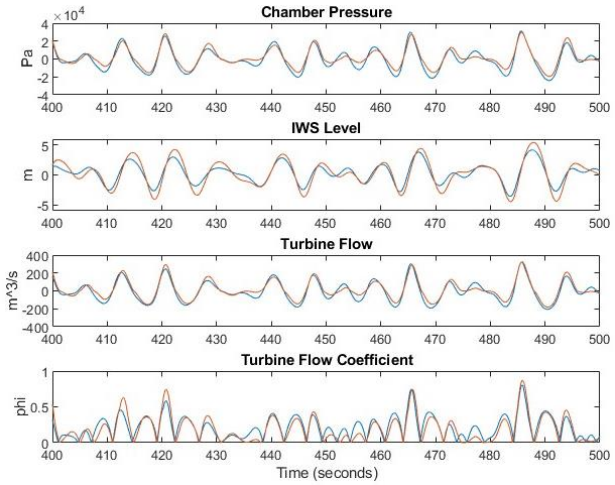

Fig. 7: Simulations for relief valve control development under sea state B05 showing chamber pressure, IWS level, Turbine Air Flow, and Turbine Flow Coefficient with relief valves non-operational (blue) and operational (orange).

Fig. 7 shows the results from simulations performed for sea state B05. In Fig. 7, the data in blue are the results from simulating the system with the valves closed and the data in orange is from simulating it with the required valves, in this case DN400 and DN600, open. Opening the two valves should result in a pressure drop of 55%. However, the results indicate minimal pressure drop, but they do show a significant increase in the movement of the internal water surface. While the results of this modelling suggest that the

relief valves are not operating as intended, small scale tank testing and prior real applications with relief valves for OWCs [2] suggest that the model is not properly simulating device response during valve operation. Further work is required to ensure that the model is properly representing real device behaviour.

I. Energy Storage System Control

As introduced in section B, the aim of the ESS is to reduce short-term fluctuations in the power feed-in to the grid. This is the focus of the early development of control for the ESS. Furthermore, a suitable sizing of the ESS had to be identified, based on this development.

The initial turbine control algorithm testing was conducted only under conditions with a significant wave height (H_s) of 3.5 m because in higher energy sea states, the relief valves will be required. However, the optimization for the valve control is still under development, and it has not yet been developed well enough to work with the ESS control. Table II again shows the sea conditions simulated when testing the ESS.

A simple controller has been developed, Fig. 8 shows the schematic of the structure. The power to be fed into or fed out of the super capacitor system (P_{2SC}) is calculated from the measured generator power, P_{gen}. This input is available in the generator-side inverter. The control aim is to charge/discharge the ESS with the fluctuating share of the generated power, while the smoothed rest of the generator power will be fed into the grid. For this, a filter is included in the left part, with time constant T_{ctrl}.

In the right-hand part, any negative value of P^*_{2SC}, i,e. any discharging power request, is multiplied by the ESS system efficiency, η_{SC}. This keeps the the state of charge of the capacitor on a constant level in average. In a further development, this state will be considered as an input to the control.

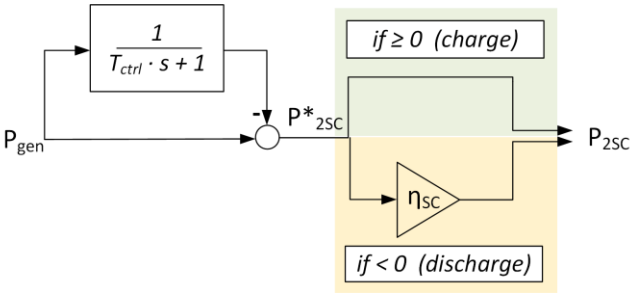

Fig. 8: Schematic of the simple control strategy to load / unload the super capacitor system in order to reduce short term fluctuations in the power feed-in to the grid.

The developed control strategy has been tested using a simple system model, in order to assess its capability to reduce the short-term power fluctuations in the feed-in to the grid.

The simulation input was the generator power as arising from sea state B12. The ESS efficiency has been assumed 90%, including its inverter losses. Note that delays due to communication, measurement and controller hardware have not yet been considered.

Two different values of T_{ctrl}., 1.5 and 2.5 have been applied, Fig. 9 and Fig. 10 show the results. Each upper diagram contains the generator power, as well as the power fed into the grid. The smoothing effect of the control can be clearly seen, where the higher the filter time constant, the stronger will be the smoothing effect.

The according power fed into /out of the capacitor system is shown in the second diagram. The bottom is the resulting available energy in the super capacitor.

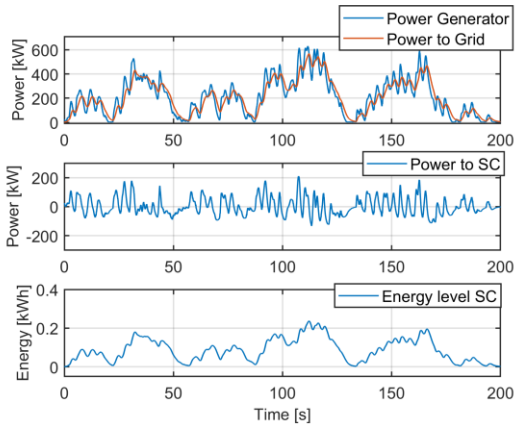

Fig. 9: Power feed-in to the grid (top), power through super capacitor (middle), and stored energy (bottom) for Sea State B12 and controller with T_{ctrl} =1.5 applied.

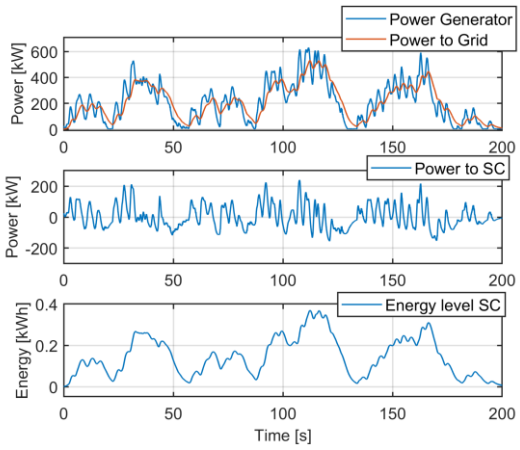

Fig. 10: Power feed-in to the grid (top), power through super capacitor (middle), and stored energy (bottom) for Sea State B12 and controller with T_{ctrl} =2.5 applied.

In order to see the effect of the capacitor system on the power quality more clearly, the power spectral density has been calculated both for the generator power and power feed-in to the grid. Fig. 11 and Fig. 12 show the results for the two controller parameters, respectively.

Comparing the two data sets in the upper diagrams of these figures, we see that in each case, the generator power fluctuations between 0.2 and 0.3 Hz (blue) are mitigated almost to zero for the feed-in to the grid (red), i.e., they are not visible in the signal. For both parameters, the fluctuations between 0.05 Hz and 0.1 Hz are additionally reduced, where the reduction is stronger with T_{ctrl}=2.5. Clearly, the super capacitor has more charging/discharging cycles in the according frequency range for T_{ctrl}=2.5, see the second diagrams of each figure.

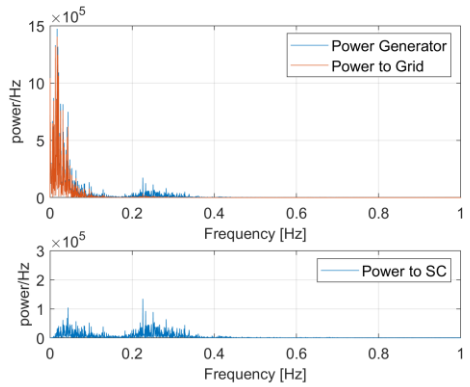

Fig. 11: Power spectral density of generator power and power feed-in to the grid with T_{ctrl}=1.5 applied.

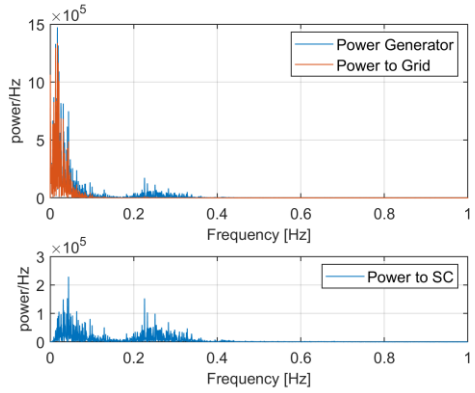

Fig. 12: Power spectral density of generator power and power feed-in to the grid with T_{ctrl}=2.5 applied.

Naturally, for T_{ctrl} = 2.5 with the stronger smoothing effect, the super capacitor system needs a higher power feed-in capability, as well a larger storage capability. These data are listed in Table VI and are the base for sizing the ESS.

TABLE VI
MAXIMUM POWER AND MAXIMUM STORED ENERGY FOR THE TWO CONTROLLER PARAMETERS, FOR SEA STATE B12

Control Strategy	PT1_T1.5	PT1_T2.5
Maximum Power (kW)	210	238
Stored Energy (kWh)	0.24	0.37

Further simulations have been carried out for sea states with both lower and higher waves than B12. They have shown that the introduced control approach will suffice for lower energy seas as well. However, at sea states with higher available energy, the storage capacity of the ESS as derived according to Table VI will not be large enough to accommodate the power swings the PTO will encounter. Further development of the control algorithms is necessary to use the same ESS sizing under those higher energy conditions.

V. CONCLUSIONS & FUTURE WORK

The results for early development and testing of the control algorithms for the various new additions to the OE35 PTO system provided mix results. The turbine and ESS control development produced effective algorithms that improved performance of both systems, and the foundational algorithms created will be key building blocks for the overall PTO control system.

The development of the relief valve control has resulted in minimal progress. The results of simulation testing of the valves using the model do not match observed results from model tank testing. These results intimate that further investigation of the hydrodynamic and pneumatic models developed for this project.

To improve the accuracy of the Simulink model, small scale tank testing will be performed on a scale model of the OE35 with the relief valve included. The data from tank testing will be used to tune the MATLAB Simulink model. After the MATLAB model is tuned, the model testing will be re-simulated, and the control algorithms will be re-evaluated and adjusted.

Additionally, to assist the aforementioned WETS project and to further evaluate the model, it will be reconfigured to match the OE35 PTO system for the upcoming WETS deployment. The data collected from the WETS deployment will be used to further verify the model. This will allow for a second opportunity to tune the hydrodynamic and pneumatic models for the WEDUSEA project.

With the planned deployment of the WEDUSEA is for summer of 2024, the development of the control algorithms for each PTO subsystem, as well as the overall control strategy will continue at pace, alongside the continued development of the model. The objective is to have the comprehensive control system for the OE35 PTO developed, tested, and operational from the first day of the deployment. Throughout the planned two-year deployment, both the model and the control algorithms will continue to be refined in parallel. The data gathered during deployment will be used to improve the model, and simulations will be utilised to continue to adjust the control algorithms as necessary. Two of the secondary outcomes of the WEDUSEA project are to have a mature and verified system model along with a proven, efficient, and robust control for the OE35. This will help reach one of the stated three primary goals of the project, which is to reduce cost and enable future deployment of multiple units within an array.

ACKNOWLEDGEMENT

Funded by the European Union and UKRI. Views and opinions expressed are however those of the author(s) only and do not necessarily reflect those of the European Union, UKRI, or CINEA. Neither the European Union nor the granting authority can be held responsible for them.

REFERENCES

[1] J. Kelly, T. Lewis and J. McCarthy, "Expected impacts of the wets deployment of the oe35 oscillating water column," in *14th European Wave and Tidal Energy Conference*, Plymouth, UK, 2021.

[2] K. Monk, D. Conley, V. Winands, M. Lopes, Q. Zou and D. Greaves, "Simulations and field tests of pneumatic power regulation by valve control using short-term forecasting at the Pico OWC.," in *The 11th European Wave and Tidal Energy Conference*, Uppsala, Sweden, 2015.

[3] K. Monk, V. Winands and M. Lopes, "Chamber pressure skewness corrections using a passive relief valve system at the pico oscillating water column wave energy plant," *Renewable Energy,* vol. 128, pp. 230-240, 2018.

[4] M. Folley and T. J. T. Whittaker, "he effect of sub-optimal control and the spectral wave climate on the performance of wave energy converter arrays," *Applied Ocean Research,* vol. 31, no. 4, pp. 260-266, 2009.

[5] R. Gervelas, F. Trarieux and M. Patel, "A time-domain simulator for an oscillating water column in irregular waves at model scale," *Ocean Engineering,* vol. 30, no. 8-9, pp. 1007-1013, 2011.

[6] J. Kelly, W. Wright, W. Sheng and K. O'Sullivan, "Implementation and verification of a wave-to-wire model of an oscillating water column with impulse turbine," *IEEE Transactions on Sustainable Energy,* vol. 7, no. 2, pp. 546-553, 2015.

[7] F. Faÿ, J. Henriques, J. Kelly, M. Mueller, M. Abusara, W. Sheng and M. Marcos, "omparative assessment of control strategies for the biradial turbine in the Mutriku OWC plant," *Renewable Energy,* vol. 146, pp. 2766-2784, 2020.

[8] M. Takao, T. Setoguchi, Y. Kinoue and K. Kaneko, "Wells turbine with end plates for wave energy conversion," *Ocean Engineering,* vol. 34, no. 11-12, pp. 1790-1795, 2007.